



UNIVERSITÀ POLITECNICA DELLE MARCHE
Repository ISTITUZIONALE

Thermo-rheological modelling of cement-bitumen treated materials in the small strain domain

This is the peer reviewed version of the following article:

Original

Thermo-rheological modelling of cement-bitumen treated materials in the small strain domain / Raschia, S.; Di Benedetto, H.; Lamothe, S.; Carter, A.; Graziani, A.; Perraton, D.. - In: TRANSPORTATION GEOTECHNICS. - ISSN 2214-3912. - STAMPA. - 31:(2021). [10.1016/j.trgeo.2021.100647]

Availability:

This version is available at: 11566/292646 since: 2024-04-29T19:46:41Z

Publisher:

Published

DOI:10.1016/j.trgeo.2021.100647

Terms of use:

The terms and conditions for the reuse of this version of the manuscript are specified in the publishing policy. The use of copyrighted works requires the consent of the rights' holder (author or publisher). Works made available under a Creative Commons license or a Publisher's custom-made license can be used according to the terms and conditions contained therein. See editor's website for further information and terms and conditions.

This item was downloaded from IRIS Università Politecnica delle Marche (<https://iris.univpm.it>). When citing, please refer to the published version.

note finali coverpage

(Article begins on next page)

Thermo-Rheological Modelling of Cement-Bitumen Treated Materials in the Small Strain Domain

Abstract

Cold recycled materials (CRM) have been introduced as structural materials in road pavement structures thanks to their significant economical and environmental benefits. Among them, cement-bitumen treated materials (CBTM) are often employed because of both contributions given by bitumen (in form of emulsion) and cement. The first confers a bituminous behaviour, whereas the second ensures good short-term performance otherwise penalized by the presence of water. Water plays a fundamental role in providing workability of the mixture at the atmospheric production temperatures. Due to such peculiarities, CBTM mixtures require attention when rheological modelling is performed in the small strain domain. This paper provides an overview on the most common rheological model applied to bituminous mixtures (2S2P1D) and the main issues related to the application to CBTM mixtures are highlighted. Afterwards, another model is proposed from the literature, the DBN model, and applied to three mixtures. The mixtures were prepared to assess the effect of the bitumen emulsion used, as well as the type of curing conditions. Results showed that the DBN model seems to be an excellent tool for not only CBTM rheological modelling in the small strain domain and it is recommended for applications in wider experimental programs.

Keywords: Cold recycling, Bitumen emulsion, Reclaimed Asphalt Pavement, Small strain domain, Rheological modelling

1 INTRODUCTION

The increasing costs related to the road industry to face the necessity of frequent maintenance and rehabilitation projects have led to the promotion of sustainable technologies characterized by substantial environmental and economic benefits. Among them, cold recycled materials (CRM) are the most promising materials for structural layers (base or subbase), due to the possibility of reusing high quantity of reclaimed asphalt and performing the production process at atmospheric temperature (ARRA, 2001, 2016; Giani et al., 2015; Lauter & Corbett, 1998; Omrani & Modarres, 2018; Stroup-Gardiner, 2011). In fact, the bitumen is used in form of bitumen emulsion or foamed bitumen, whereas the workability of the mixtures is ensured by the addition of water (Asphalt Academy, 2009). A specific type of CRM materials is the cement-bitumen treated materials (CBTM), where the short and long-term properties are improved by the addition of ordinary Portland cement. Such materials show a dual behaviour (asphalt-like and cement-like) when bitumen and cement are employed at almost the same dosages (between 1 and 3%) (Bocci et al., 2011; Cardone et al., 2014; Chen et al., 2020; Grilli et al., 2012). In addition to the low amount of bituminous binder and the presence of cement, an important difference between CBTM and the traditional hot mix asphalts (HMA) is the use of reclaimed asphalt pavement (RAP) as a black rock (Raschia et al., 2019). The RAP is generally employed in high amount in the CBTM aggregate gradation and it is reasonable to assume that, at atmospheric temperature, the aged binder coating the aggregate particles does not blend with the added virgin binder (emulsion or foam).

In the literature, mechanical characterization of CBTM mixtures is commonly performed by means of traditional tests, often empirical, determining the resistance at high deformations (failure) (Dal Ben & Jenkins, 2014; Graziani et al., 2018; Hodgkinson & Visser, 2004; Kim et al., 2011; Zhu et al., 2019). Only few feedbacks can be found on CBTM (or CRM) mixtures characterization in the small strain domain (Chomicz-Kowalska & Maciejewski, 2020; Gandi et al., 2017; Godenzoni et al., 2015; Godenzoni et al., 2016; Saleh, 2007), even though in many cases sigmoidal functions characterized by experimental parameters are preferred instead of rheological models composed by specific elements (springs and/or dashpots) (Graziani et al., 2020). In particular, the determination and modelling of rheological properties, such as complex modulus and phase angle, allow a better understanding of the material behaviour by means of the application of a valid rheological model. In case of bituminous mixtures, the Huet-Sayegh model was widely used in the past, even though it does not allow to well represent the material behaviour at very low

frequencies (or very high temperatures) (Olard & Di Benedetto, 2003; Pronk, 2006). For this reason, the 2S2P1D was introduced to obtain a complete rheological description of bituminous mixtures and binders in the linear viscoelastic field (Olard et al., 2003). Of course, the application of this model is valid in any case where the loading conditions (number of cycles, strain amplitude, temperature) keep the material in the linear domain. When non-linearities are present, a more versatile model can be used, like the DBN model (Di Benedetto, Mondher, et al., 2007). In fact, the DBN model can be applied depending on the strain level and the formulation can be quite simple (in case of linear viscoelasticity) or more complex (permanent deformation or fatigue).

The **main** objective of this paper is to define and employ a suitable rheological model to investigate the properties of CBTM mixtures in the small strain domain. The most common models proposed by the literature **are described, highlighting** the main issues observed. **Furthermore, as a preliminary and validation step, the new approach is applied to a limited number of specimens.**

2 THERMO-RHEOLOGICAL MODELLING OF HMA AND CBTM

The main characteristic of CBTM mixtures **is the presence of both bitumen and cement as binding agents.** The contribution of both binding agents makes the thermo-mechanical and rheological description of such materials different from the traditional approaches followed for HMAs. In fact, CBTM mixtures could be considered as an intermediate material **between bitumen-stabilized mixtures, cement treated mixtures and bituminous mixtures** (Grilli et al., 2012). Rheological models developed so far are suitable for systems where the dissipation at small strain level can be explained when considering LVE behaviour. This assumption is considered valid probably because HMA are characterized by higher effective bitumen content and lower voids when compared to CBTM mixtures. For these mixtures, the aggregates are not completely coated by the bitumen film, which is instead dispersed irregularly, and the use of RAP as a black rock implies the presence of the aged binder in addition to the virgin binder (Asphalt Academy, 2009). Such considerations can explain, at a local scale, the observed behaviour during rheological testing and must be taken into account for the rheological modelling of CBTM mixtures.

The linear viscoelastic Huet-Sayegh model is a rather good tool to represent the rheological properties of bituminous mixtures but not binders, especially at low frequencies (or high temperatures). The analytical expression of the Huet-Sayegh complex modulus is described in Eq. (1):

$$E_{HS}^*(i\omega\tau_E) = E_{00} + \frac{E_0 - E_{00}}{1 + \delta(i\omega\tau_E)^{-k} + (i\omega\tau_E)^{-h}} \quad (1)$$

where i is the complex number defined as $i^2 = -1$, ω is the pulsation defined as $\omega = 2\pi f$, f is the frequency, k and h are constant exponents ($0 < k < h < 1$), δ is a constant, E_{00} is the static modulus for $\omega \rightarrow 0$, E_0 is the glassy modulus when $\omega \rightarrow \infty$, and τ_E is the characteristic time, which is the only parameter depending on the temperature.

$$\tau_E(T) = a_T(T) \cdot \tau_{0E} \quad (2)$$

where $a_T(T)$ is the shift factor at a temperature T , $\tau_E(T) = \tau_{0E}$ at the reference temperature T_0 and $\tau_E(T)$ is determined at each isotherm by minimizing the error between the measured and modelled norm of the complex modulus, $|E^*|$.

It was recently observed that applying the Huet-Sayegh model to CBTM and focusing the fitting on the $|E^*|$ led to a systematic error in the modelling of the phase angle (φ), parameter characterizing the viscous energy dissipation (Graziani et al., 2020). In particular, a constant phase lag independent of temperature and frequency was observed between the modelled and experimental values, stressing the fact that the model underestimates the total energy dissipation considering only the viscous component. As a result, it seemed that CBTM mixtures are characterized by a total energy dissipation composed of a viscous component and non-linear phenomena (non-viscous). The authors described this aspect as energy dissipation probably due to the aggregate-to-aggregate contact and friction. As a solution, they proposed an analytical modification to the Huet-Sayegh equation, which consists in the addition of a constant phase angle and expressed by Eq. (3).

$$E_{HSq}^*(i\omega\tau_E) = E_{HS}^*(i\omega\tau_E) \cdot \exp\left(iq\frac{\pi}{2}\right) \quad (3)$$

where $E_{HS}^*(i\omega\tau_E)$ is the Huet-Sayegh model (Eq. (1)) and the term $\exp\left(iq\frac{\pi}{2}\right)$ represents an additional dissipation element with an angle, φ_{AEP} , equal to $q\frac{\pi}{2}$ without affecting the absolute value of the complex modulus.

Such correction led to a better fitting of the experimental data obtained for CBTM mixtures, but in this form, the model is only suitable for sinusoidal loading and cannot be used to extend the material representation in the time domain for another loading path. This drawback does not exist for the DBN model presented below. In the literature, the 2S2P1D model is extensively used to describe the rheological behaviour of bituminous mixtures in the LVE field with good approximation. In addition, the parameters that define the 2S2P1D model are used in the calibration process of the DBN model.

2.1 2S2P1D model

The 2S2P1D model is a linear viscoelastic rheological model composed of 2 springs, 2 parabolic elements and 1 dashpot. In particular, one spring is placed in parallel with a series of the remaining elements (Figure 1). Thanks to its nature, this model is largely employed to model unidimensional or tridimensional behaviour of bituminous materials (binders, mastics and mixtures) (Di Benedetto, Delaporte, et al., 2007; Di Benedetto et al., 2004; Tiouajni et al., 2011). The analytical expression of the complex modulus in the 2S2P1D model is given in Eq. (4) for a fixed reference temperature:

$$E_{2S2P1D}^*(i\omega\tau_E) = E_{00} + \frac{E_0 - E_{00}}{1 + \delta(i\omega\tau_E)^{-k} + (i\omega\tau_E)^{-h} + (i\omega\beta\tau_E)^{-1}} \quad (4)$$

where some parameters are already explained, and β is a parameter linked to the dashpot viscosity $\eta = (E_0 - E_{00})\beta\tau$ when $\omega \rightarrow 0$.

As already mentioned, this model is particularly suitable for bituminous mixtures or materials with almost only viscous dissipation and with seven constants can fully describe the rheological behaviour of HMA mixtures. However, it is possible that, in case of CBTM mixtures, the 2S2P1D is not able to well represent the material behaviour.

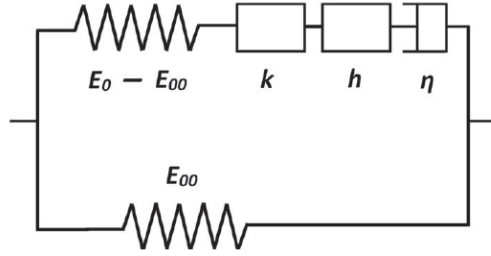


Figure 1 2S2P1D analogical representation (taken from (Gayte et al., 2016))

Analyzing the model parameters in the literature, it is observed that E_0 and E_{00} are significantly different between HMA and CBTM mixtures (Carret et al., 2018; Gandi et al., 2017; Lamothe et al., 2017). In fact, springs stiffness depends mainly on the aggregate skeleton and the air voids content. In general, E_0 in CBTM mixtures is lower than in HMA due to the higher air voids and the lower bitumen dosage. On the other hand, the value of E_{00} in CBTM mixtures is usually higher than in HMA due to the presence of cement, which constitutes a stiffening phase also at very high temperatures (or very low frequencies), when the bitumen phase is considered as fluid. Moreover, the dashpot viscosity and the related parameter β is around 10 times higher in CBTM than in HMA, indicating the small role played by the dashpot when cement is used with bitumen.

2.2 DBN model

The DBN model (named after the authors Di Benedetto and Neifar) was specifically proposed to introduce non-linearity phenomena and to describe large-strain plastic behaviour of granular soils (Blanc et al., 2011; Di Benedetto et al., 2014). Later, its application was extended to analyze plastic dissipation phenomena in bituminous mixtures (Di Benedetto, Mondher, et al., 2007; Gayte, 2016; Neifar & Di Benedetto, 2001). In the model, the non-linearity is represented by means of elastoplastic (EP) bodies in series with viscous dashpots, the latter representing the time-temperature dependency. The combination is then repeated n times (n elements) in order to increase the model precision (Figure 2a). When the strain level tends to 0, the DBN model takes its asymptotic form as a Generalized Kelvin-Voigt (GKV), and the EP bodies are replaced by springs (Figure 2b). When the number of elements tends to the infinite, the representation passes from a discrete spectrum to a continuous spectrum. Thanks to the high versatility, this model is able to describe behaviour for a wide range of solicitations, temperatures and cycle numbers.

The EP bodies, which represent a non-viscous behaviour, are generally adopted for non-cohesive (or elastoplastic) granular materials (Ashmawy et al., 1995; Blanc et al., 2011; Di Benedetto et al., 2014; Tatsuoka et al., 2008). Plastic dissipation can be observed in sands for cycles at small strain amplitude, characterized by a hysteretic stabilized behaviour. Considering materials composed of aggregates and bituminous binder, the non-viscous behaviour should be attributed to aggregates (or RAP in this case), whereas the viscous contribution to the binder. With such considerations, it can be assessed that the non-viscous behaviour is independent from temperature (and frequency, if the Time-Temperature Superposition Principle stands), which is instead affecting the purely viscous part. In case the DBN model is applied to represent plasticity phenomena at small cycles number (and small strain domain), it can take a simplified form (Attia, 2020).

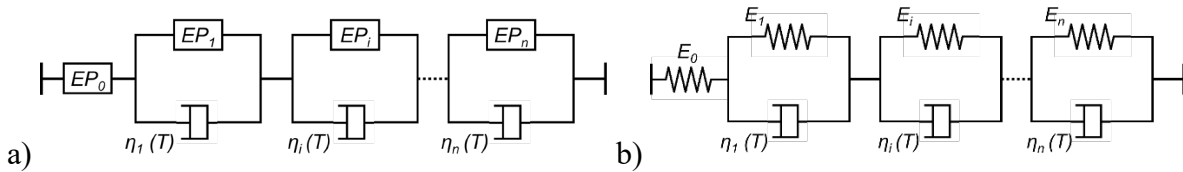


Figure 2 a) DBN model for bituminous mixtures; b) Generalized Kelvin-Voigt model, which gives an asymptotic representation of the DBN model when strain tends to 0

The cyclic response of EP bodies is characterized by a function linking the strain and the stress, called “virgin curve” (Figure 3). One property of this function is that the unloading (or loading) curve joins tangentially the virgin unloading (or loading) curve at the inverse value of the reversal stress (Di Benedetto, Mondher, et al., 2007).

For many construction materials, including metals, concrete and soils, the dissipation behavior may be expressed by the specific damping capacity ψ , which, for the KV body and small dissipation energy, is calculated as follows (Genta, 2009):

$$\psi = \frac{\Delta W_{LVE}}{W_E} = \frac{\pi \varepsilon_0 \sigma_0 \sin \phi}{1/2 \varepsilon_0 \sigma_0} = 2\pi \sin \phi \quad (5)$$

where ΔW_{LVE} is the area of the hysteresis loop with elliptical shape (energy dissipated at each cycle), W_E is the energy stored by the spring at each cycle, ε_0 is the amplitude of the sinusoidal

strain, σ_0 is the amplitude of the sinusoidal stress and φ is the frequency-dependent phase angle describing the lag between stress and strain in the linear viscoelastic response.

The EP bodies store elastic energy and dissipate through time-temperature independent mechanisms. As a result, a sinusoidal loading is represented by an hysteresis loop as in Figure 3.

The energy ΔW_{EP} dissipated by the EP body is computed as:

$$\Delta W_{EP} = W_{EP}\psi = 1/2 \varepsilon_0 \sigma_0 \psi = 2\pi D \varepsilon_0 \sigma_0 \quad (6)$$

where $D = \psi/4\pi$ is an adimensional time-temperature independent damping ratio.

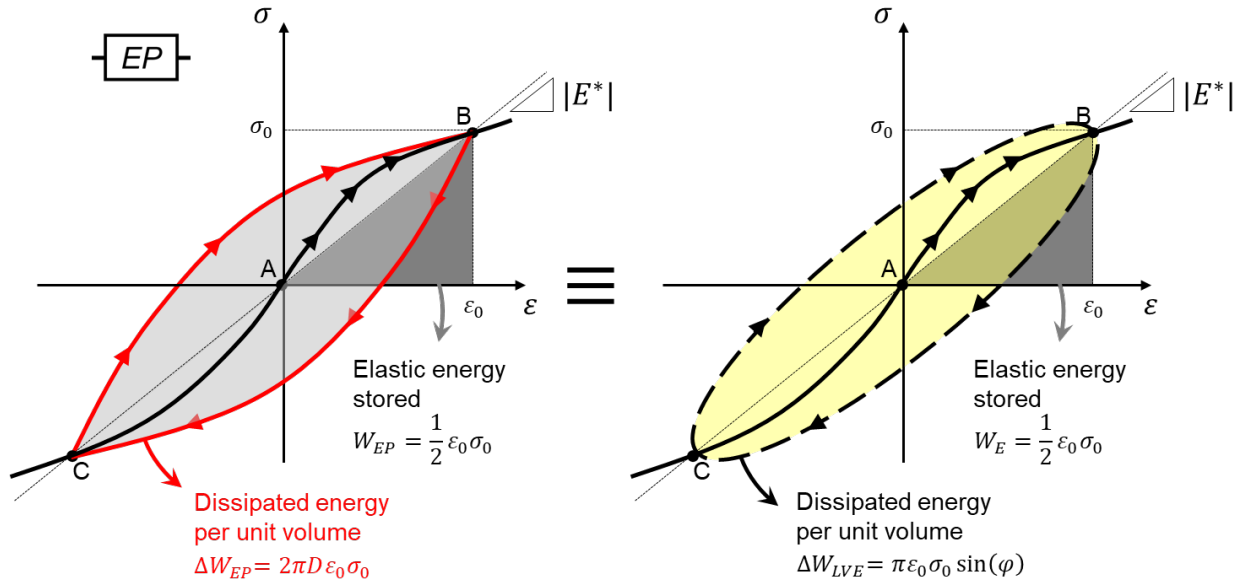


Figure 3 Cyclic loading behaviour of elastoplastic element for small number of cycles (path ABCB)

In case the number of cycles applied and the deformation are small, the plastic energy dissipation ΔW_{EP} can be expressed as an equivalent linear viscoelastic dissipation ΔW_{LVE} through the definition of an equivalent phase angle, by fixing $\Delta W_{EP} = \Delta W_{LVE}$ (Figure 3):

$$\sin(\varphi_{EP}) = 2D \quad (7)$$

The version of the DBN model presented in this paper is obtained by the series arrangement of units consisting of a viscous and temperature-dependent dashpot $\eta_i(T)$ in parallel with a EP_i

body (E_i, D_i). Moreover, the dashpot is not present in the first unit ($\eta_0 = 0$) and all units are characterized by the same dissipation parameter ($D_i = D$) (Figure 4).

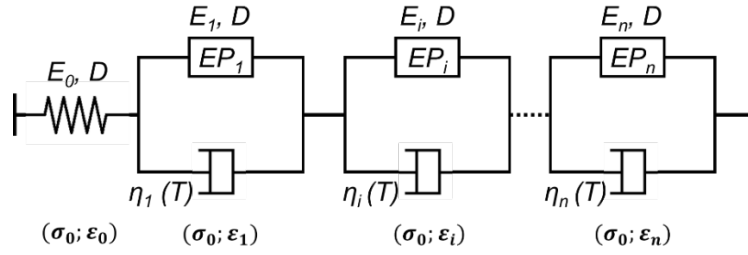


Figure 4 Representation of the DBN model applied in the small strain domain, EP are represented by a spring (modulus, E) and a non-viscous dissipation (D)

As a consequence, the DBN model phase angle φ_{DBN} is expressed as the total contribution by the viscous and non-viscous components (Figure 5):

$$\sin(\varphi_{\text{DBN}}) = \sin(\varphi_{\text{LVE}} + \varphi_{\text{EP}}) = \frac{\Delta W_{\text{DBN}}}{\pi \varepsilon_0 \sigma_0} = \frac{\Delta W_{\text{LVE}} + \Delta W_{\text{EP}}}{\pi \varepsilon_0 \sigma_0} = \sum_{i=0}^n \left(\frac{\omega \eta_i}{E_i^2 + (\omega \eta_i)^2} + \frac{2 \cdot D \cdot E_i}{E_i^2 + (\omega \eta_i)^2} \right) \cdot |E^*| \quad (8)$$

where ΔW_{DBN} is the total cycle dissipation (viscous and non-viscous), E_i and η_i are the Young's modulus and the Newtonian viscosity of the i^{th} element, respectively, ω is the pulsation, φ_{LVE} is the phase angle of the viscous dashpot, φ_{EP} is the phase angle of the non-viscous damping, and D is the damping ratio (Ashmawy et al., 1995).

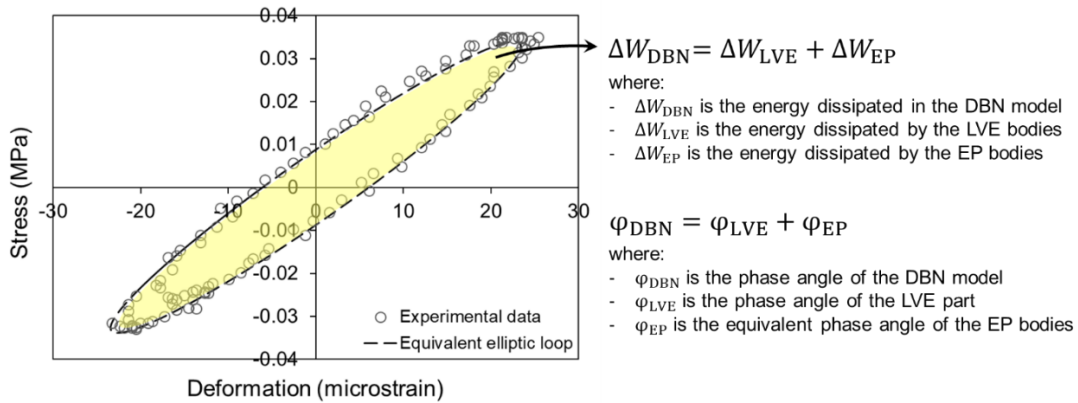


Figure 5 Energy dissipation during cyclic loading in the small strain domain (experimental data superposed to an equivalent sinusoidal loading)

It is assumed that the addition of non-viscous dissipation does not influence the value of the complex modulus, which can be expressed from the GKV configuration:

$$E_{GKV}^*(i\omega, T) = \left(\frac{1}{E_0} + \sum_{i=1}^n \frac{1}{E_i + i\omega\eta_i(T)} \right)^{-1} \quad (9)$$

where i , ω and T were previously explained, E_0 is the Young's modulus of the first element, E_i and η_i were previously explained. The number of elements n can be chosen arbitrarily to reduce the distance between the discrete GKV configuration and the 2S2P1D. In particular, the 2S2P1D model should be initially fitted on the norm of the complex modulus of the material, and then the GKV model is calibrated according to the 2S2P1D (Figure 6).

Consequently for any chosen number of elements (n), the DBN model only needs seven constants from 2S2P1D plus an additional parameter (φ_{EP}) to take into account plasticity at small strain levels.

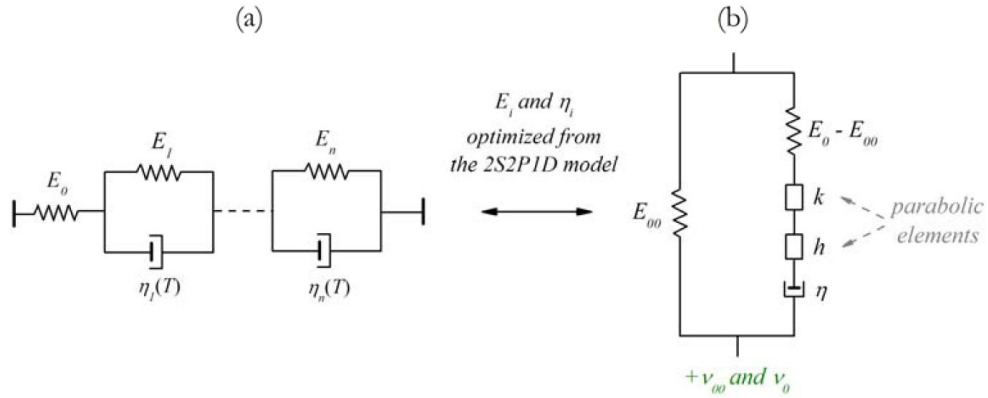


Figure 6 Correlation between: a) GKV model, and b) 2S2P1D model (taken from (Di Benedetto, Delaporte, et al., 2007))

3 MATERIALS AND METHODOLOGY

3.1 Materials and mixtures

The CBTM mixtures produced for this study are characterized by an aggregate distribution composed of 94% of RAP and 6% of limestone filler. The correction with filler allows having a gradation close to the maximum density curve (Figure 7). The properties of the RAP aggregate are

listed in Table 1. The ordinary Portland cement dosage was fixed at 1.5% by mass of dry aggregates. The cement was a GU type (standard CSA A3000) with compressive strength at 28 days of 43.9 MPa (standard ASTM C109).

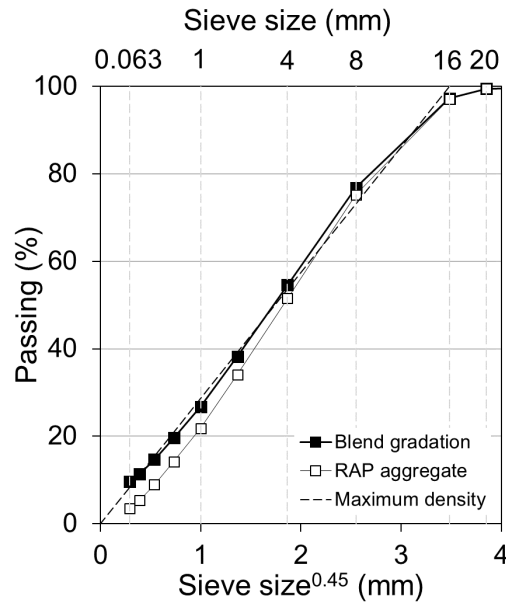


Figure 7 Maximum density curve, RAP and blend gradations

Table 1 RAP aggregate properties

Property	Standard	Unit	Value
Binder content	ASTM D6307	%	5.5
Nominal maximum particle dimension	ASTM D448-03	mm	16
Maximum specific gravity	ASTM C127-128	-	2.482
Average bulk density	LC 21-065, -066 and -067	-	2.323
Water absorption	ASTM C127 and C128	%	1.1

Table 2 Bitumen emulsions properties

Bitumen emulsion properties	Standard	Unit	Emu. A	Emu. B
Density	ASTM D6397-16	g/cm ³	1.0	n.d.*
Viscosity @ 40 °C	EN 13302	s	N/A	42.5
Residual bitumen content	EN 1428 or ASTM D6997-12	%	60.3	60.0
Storage stability @ 24 hours	ASTM D6930-10	%	0.6	n.d.*
Breaking Index	EN 13075	%	n.d.*	2
Residual bitumen properties				
Penetration @ 25 °C	EN 1426 or ASTM D5-13	mm	4.1	10.0
Softening point	EN 1427 or ASTM D36-14	°C	48.6	43.0
*n.d.: not determined				

Mixtures were produced with two bitumen emulsions in order to compare two different bitumen sources. The main properties of both emulsions are listed in Table 2, and they are named from now on as Emulsion A and Emulsion B.

In both cases, the bitumen emulsion dosage was fixed at 5% (3% of residual bitumen) by mass of aggregates. The total water dosage was fixed at 4.0% by mass of aggregate, in order to reach the target air voids of 15% without employing high compaction energy and to avoid any material loss (water, bitumen and/or fine particles) during compaction.

3.2 Mixtures production

After mixing, the specimens were compacted by means of a gyratory compactor (GC) with mould diameter of 100 mm, constant pressure of 600 kPa, gyrations rate of 30 rpm and internal angle of 1.16°. The volumetric composition of the specimen is monitored with compaction, which is performed at fixed height to obtain the target value of voids in the mixture (V_m) of 15% ± 1% (Grilli et al., 2016):

$$V_m = \frac{V_{V,A} + V_{W,I}}{V} \cdot 100 = \frac{V - (V_S + V_C + V_{B,R})}{V} \cdot 100 \quad (10)$$

where V is the total volume of the specimen, V_S is the bulk volume of aggregates (in saturated surface dried condition), V_C is the volume of cement, $V_{B,R}$ is the volume of residual bitumen from emulsion, $V_{W,I}$ is the volume of intergranular water and $V_{V,A}$ is the volume of air. A total of nineteen (19) specimens were produced, but only three (3) are considered in this study to focus the attention on the proposed model and its description.

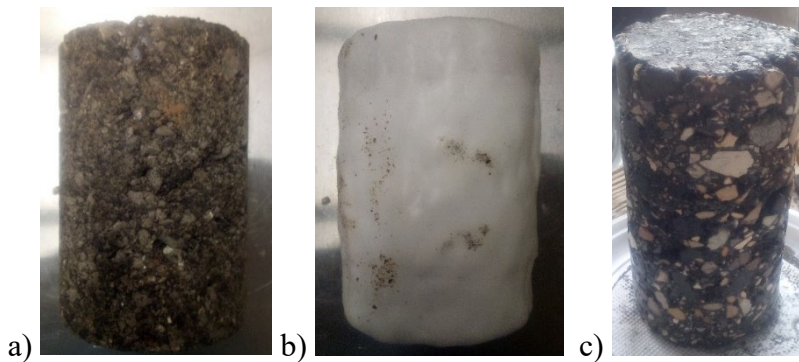


Figure 8 SGC specimen of Ø100 mm x 140 mm: a) un-sealed condition, b) sealed condition and, c) coring and sawing to obtain the testing specimens of Ø75 x 120 mm

After compaction, the specimens followed a curing process as shown in Table 3 (Raschia et al., 2020). The period lasted 1 year, simulating a long-term curing to reach a quite stable condition of the physical and mechanical properties. The first and second curing periods, for a total of 28 days, was same for the three specimens. After that, two specimens were kept in unsealed conditions for the third curing period, whereas one specimen was wrapped in plastic foil and sealed with several layers of wax for a final coating thickness of around 5 mm. The sealed condition after 28 days was chosen to stop the curing and/or ageing of the material, which instead was promoted in the unsealed specimens. At the end of the third curing period, the three specimens were cored at a diameter of 75 mm and prepared for complex modulus testing (Figure 8).

Table 3 Mixtures naming and curing process

Emulsion	Mixture	Curing types		
		1 st	2 nd	3 rd
		14 days	14 days	11 months
A	A Unsealed	25 °C	40 °C ⁽¹⁾	Room temperature (Unsealed)
	A Sealed			Room temperature (Sealed)
B	B Unsealed		40 °C	Room temperature (Unsealed)

⁽¹⁾ The curing was performed with controlled relative humidity at 55 ± 5 %

3.3 Experimental devices

The experimental program was carried out in two laboratories with different equipments, as a collaboration between different institutions. However, it is assumed that testing apparatus does not significantly influence results as long as the test is performed in the LVE field and with same testing conditions (tension-compression). In case of mixtures with Emulsion A, specimens were tested with an MTS press, whereas specimen with Emulsion B was tested with an asphalt mixture performance tester pro (AMPT PRO) servo-hydraulic press. However, complex modulus tests were performed in both cases in only compression configuration (haversine loading) and the axial strain was measured by placing three extensometers in the middle part of the specimen and 120° apart (Figure 9). The target axial strain was 50 and 30 microstrain for Emulsion A and Emulsion B mixtures, respectively. Specimens with Emulsion A were tested at a temperature range between -20 °C and 40 °C with 10 °C steps, while frequencies ranged between 0.1 Hz and 10 Hz. In case

of Emulsion B, temperature ranged between 0 °C and 40 °C with 10°C steps, and frequencies varied between 0.1 Hz and 10 Hz.

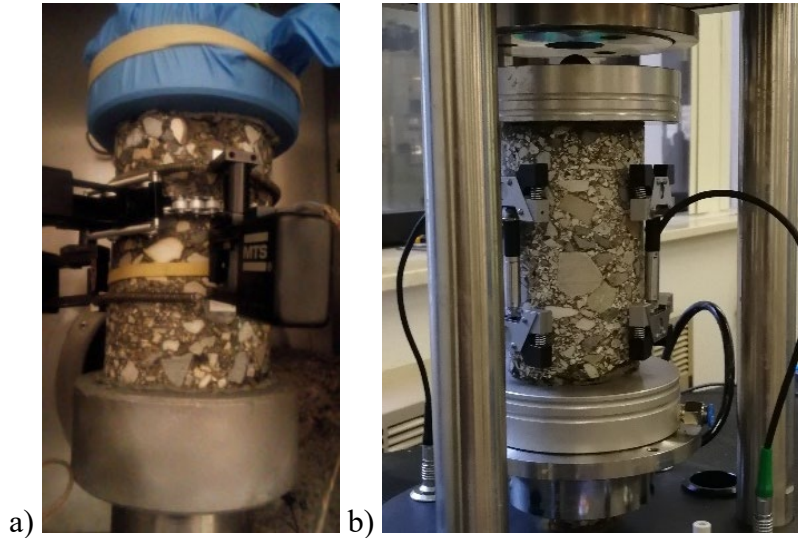


Figure 9 View of a specimen with measurement system in: a) MTS press and, b) AMPT PRO press

4 RESULTS ANALYSIS

Figure 10 shows results from the tested mixtures in the Cole-Cole plan and Black space. It can be observed that in all the cases the experimental points follow a continuous line, indicating that the Time-Temperature Superposition Principle (TTSP) is respected and the rheological models described above can be applied. The range of $|E^*|$ values is quite the same for the three mixtures studied indicating that the emulsion type and the type of curing did not significantly affect the stiffness of the mixtures (Figure 10b). On the contrary, it can be observed that mixture B_Unsealed is characterized by a different trend of the phase angle when compared to both mixtures with Emulsion A (Figure 10b). It is reasonable to expect that changing the emulsion, and hence the residual binder, the viscous properties could have been affected. Moreover, comparing the two mixtures, A_Unsealed and A_Sealed, it is noted that the experimental points are superposed and a distinction is not possible. Therefore, the sealing condition during the third stage of curing did not have a clear effect on mixtures produced with Emulsion A, since the material properties did not change as expected (no further curing and apparently no ageing).

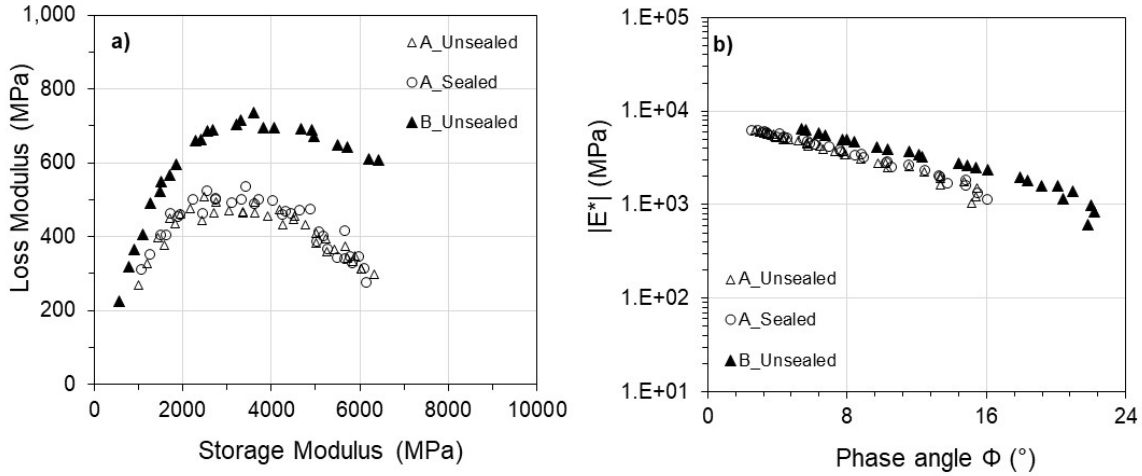


Figure 10 Experimental results showed in: a) Cole Cole plan and, b) Black space

4.1 Time-Temperature Superposition Principle, TTSP

The experimental data show that the TTSP is applicable to CBTM mixtures. As a consequence, the isothermal curves of the norm of the complex modulus, $|E^*|$, and of the phase angle, ϕ , can be shifted in order to obtain the respective master curves (Figure 11).

Figure 11 shows the master curves of the norm of the complex modulus and phase angle at a reference temperature $T_{ref} = 20^\circ\text{C}$. As in the previous representation, the effect of the emulsion is highlighted on the mechanical properties of mixtures studied. In particular, mixture B_Unsealed showed lower modulus at low frequencies (or high temperatures) and higher modulus at high frequencies (or low temperatures), confirming the crucial role of the bituminous binder used in the thermal sensitivity of the mixture. Such effect is also visible in the master curve of the phase angle, which is globally higher for mixture with Emulsion B compared to mixtures with Emulsion A (Figure 11b). Considering that the dosage of residual bitumen is the same, this difference could be explained by the fact that the bitumen from Emulsion B is more time-temperature dependant than bitumen from Emulsion A.

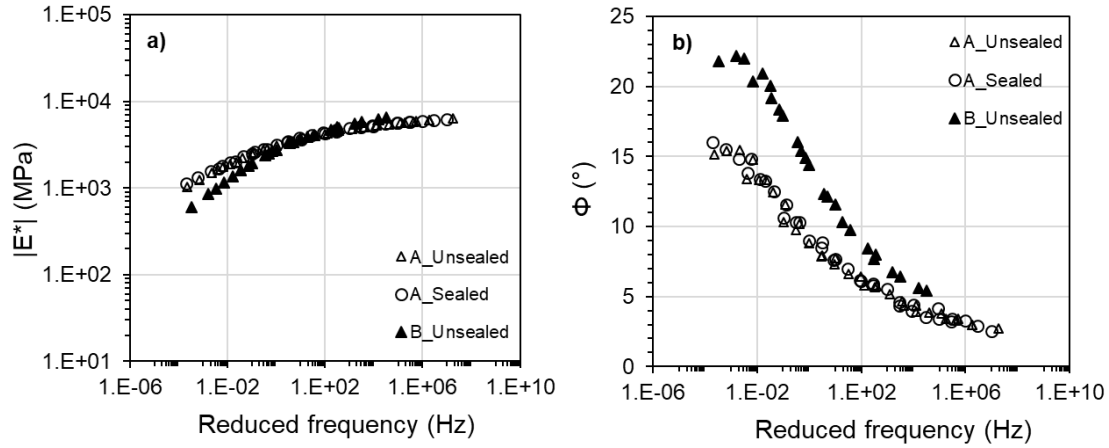


Figure 11 At $T_{ref} = 20\text{ }^{\circ}\text{C}$, master curves of: a) The norm of the complex modulus $|E^*|$ and, b) The phase angle ϕ

Figure 12 shows the shift factors in function of the temperature. The experimental points are modelled by the Williams–Landel–Ferry (WLF) model, mathematically expressed as:

$$\log(a_T) = -\frac{C_1(T-T_S)}{C_2+T-T_S} \quad (11)$$

where a_T is the shift factor, C_1 and C_2 are constants, T is the temperature and T_S is the reference temperature (Ferry, 1980). It is observed that the shift factors of the three mixtures are significantly close at all the temperatures tested (Table 4). The obtained values of a_T can be compared to the ones obtained for HMA mixtures in the literature, tested in the same range of temperatures (Di Benedetto et al., 2004). Moreover, such dependency on temperature highlights the thermo-mechanical response of CBTM mixtures. It has been shown that in HMA the a_T coefficients are very close between the binder and the related mixture (Di Benedetto et al., 2004). Hence, assuming this is also valid for CBTM, it would be possible to have the same shift factors for both residual bitumen of the emulsions used.

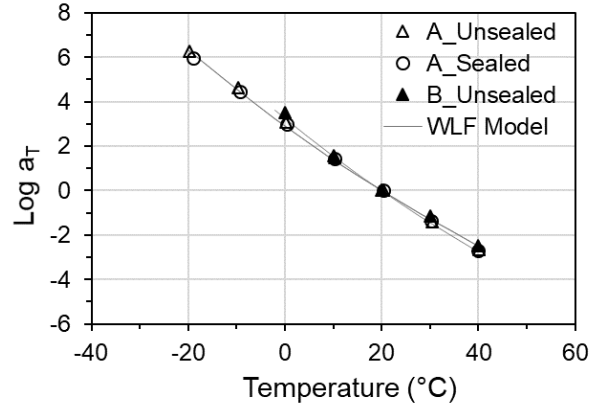


Figure 12 Shift factors, a_T , and WLF model related to the studied mixtures

Table 4 WLF parameters

Parameters	A Unsealed	A Sealed	B Unsealed
C_1	34.7	34.7	38.7
C_2	258.5	258.5	258.2

4.2 The 2S2P1D model

Figure 13 shows the experimental data obtained for one mixture (B_Unsealed) modelled with the 2S2P1D model. According to the LVE theory for bituminous materials, if the TTSP is respected, the rheological model should be unique and valid in all the representations: master curves, Black space and Cole-Cole plan. In Figure 13, three calibrations of the 2S2P1D model are presented:

- optimization from the data in the Cole-Cole and Black spaces, minimizing the error $|\Delta E^*|$ as in Eq. (12) (named: 2S2P1D_CC+BS);
- optimization from the data plotted in the master curve of the $|E^*|$, minimizing the error $\text{dev } |E^*|$ as in Eq. (13) (named: 2S2P1D_ $|E^*|$);
- optimization from the master curve of ϕ minimizing the error $\Delta\phi$ as in Eq. (14) (named: 2S2P1D_ ϕ).

$$|\Delta E^*| = \sqrt{(E_{1,\text{exp}} - E_{1,2\text{S2P1D}})^2 + (E_{2,\text{exp}} - E_{2,2\text{S2P1D}})^2} \quad (12)$$

$$\text{dev } |E^*| = \frac{|E^*|_{\text{exp}} - |E^*|_{2\text{S2P1D}}}{|E^*|_{\text{exp}}} \cdot 100 \quad (13)$$

$$\Delta\phi = \phi_{\text{exp}} - \phi_{2\text{S2P1D}} \quad (14)$$

where $E_{1,\text{exp}}$ and $E_{1,2\text{S2P1D}}$ are the storage moduli of the experimental results and the 2S2P1D model, respectively; $E_{2,\text{exp}}$ and $E_{2,2\text{S2P1D}}$ are the loss moduli of the experimental results and the 2S2P1D model, respectively; $|E^*|_{\text{exp}}$ and ϕ_{exp} are the experimental results of the norm of the complex modulus and the phase angle, respectively; $|E^*|_{2\text{S2P1D}}$ and $\phi_{2\text{S2P1D}}$ are the 2S2P1D values of the norm of the complex modulus and the phase angle, respectively.

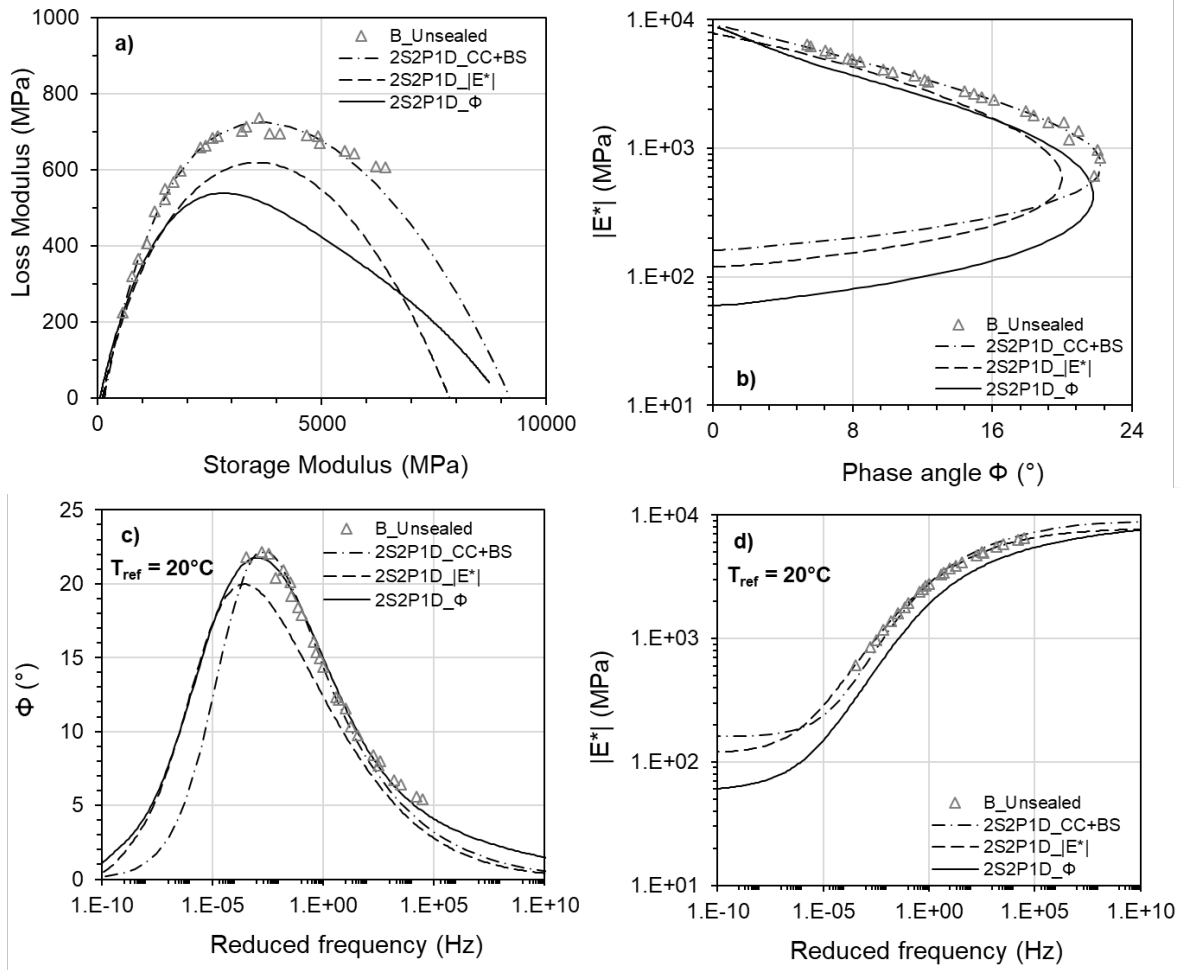


Figure 13 Optimization of the 2S2P1D model for B_Unsealed mixture according to: a) Cole-Cole plan, b) Black space, c) phase angle master curve and, d) complex modulus master curve ($T_{\text{ref}} = 20^\circ\text{C}$)

In Figure 13, it is observed that none of the three optimizations superpose among them and with the experimental data in all the four representations. The calibration 2S2P1D_CC+BS does not well represent the master curves trend at both low and high reduced frequencies (high and low

temperatures, Figure 13c-d). Furthermore, the optimization 2S2P1D_ Φ done on the phase angle master curve significantly underestimates the norm of the complex modulus, $|E^*|$, visible in the three other representations (Figure 13a-b-d). However, the model 2S2P1D_ $|E^*|$ calibrated on the master curve of the $|E^*|$ underestimates the ϕ of a constant value on the full frequencies range (around 2°, Figure 13c). This result can be justified by the presence of a non-viscous dissipation which cannot be taken into account with a LVE rheological model such as 2S2P1D. As a consequence, the results from the three mixtures studied are modelled fitting the 2S2P1D on the norm of the complex modulus (calibration : 2S2P1D_ $|E^*|$) (Figure 14). It is observed that the phase angle master curve is not well represented for all the mixtures and this is visible also in Black space and Cole-Cole plan (Figure 14a-b). For this reason, the DBN model should be applied to consider also the non-viscous contribution in the complex behaviour. The shifting was done by means of a closed-form shifting (CFS) algorithm which minimizes the area between two successive isothermal curves of $|E^*|$ and estimates the shift factors (Gergesova et al., 2011).

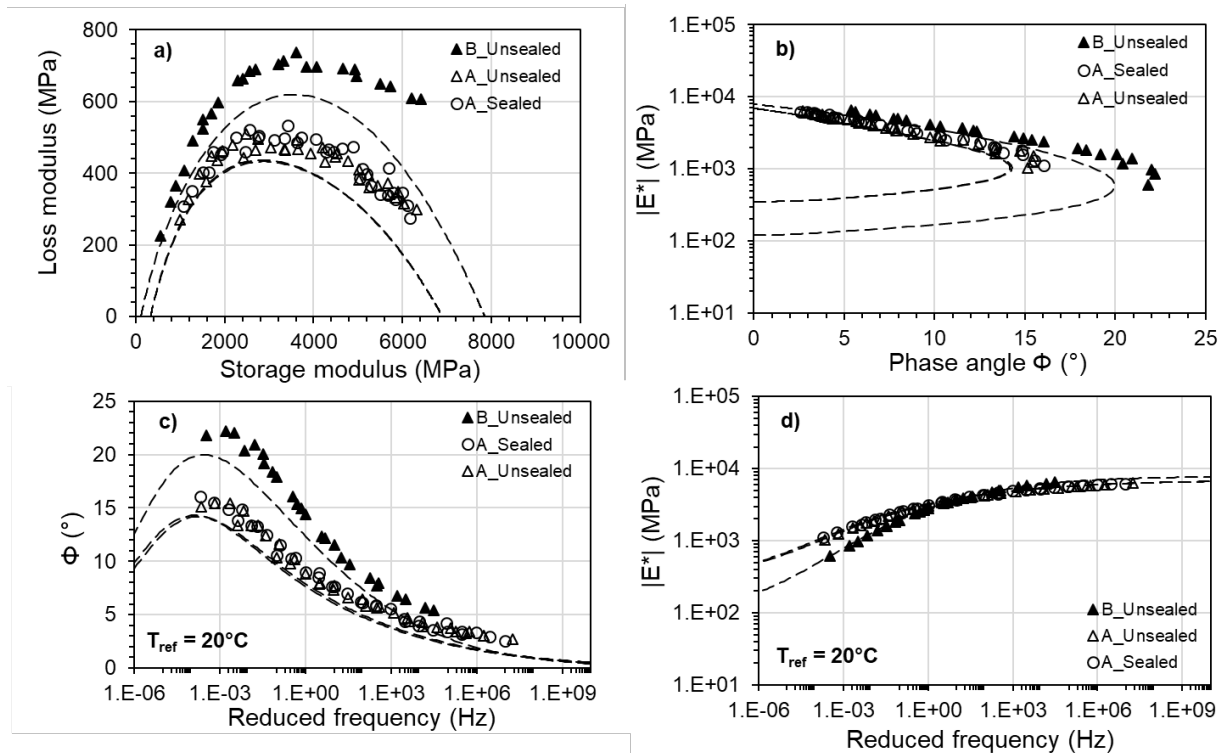


Figure 14 Application of 2S2P1D model fitted on the master curve of the norm of the complex modulus (calibration : 2S2P1D_ $|E^*|$) for: a) Cole-Cole plan, b) Black space, c) phase angle master curve and, d) complex modulus master curve ($T_{ref} = 20\text{ °C}$)

4.3 The DBN model

Figure 15 shows the experimental results of the three studied mixtures modelled with the 2S2P1D and DBN models. In order to obtain a good level of precision and correlation with the 2S2P1D, the number of elements in the GKV model was fixed at 40. The values of E_i and η_i for each element of the model are listed in the appendix A (Table A.1). It can be observed that the two models are superposed in the plan of the norm of the complex modulus (Figure 15a), whereas in the other plans the difference between the two models is due to the introduction of an equivalent phase angle representing the non-viscous dissipation, φ_{EP} . This additional parameter is visible as a shifting of the model in the Black space and phase angle master curve, and as a rotation in the Cole-Cole plan (Figure 15a-b-c).

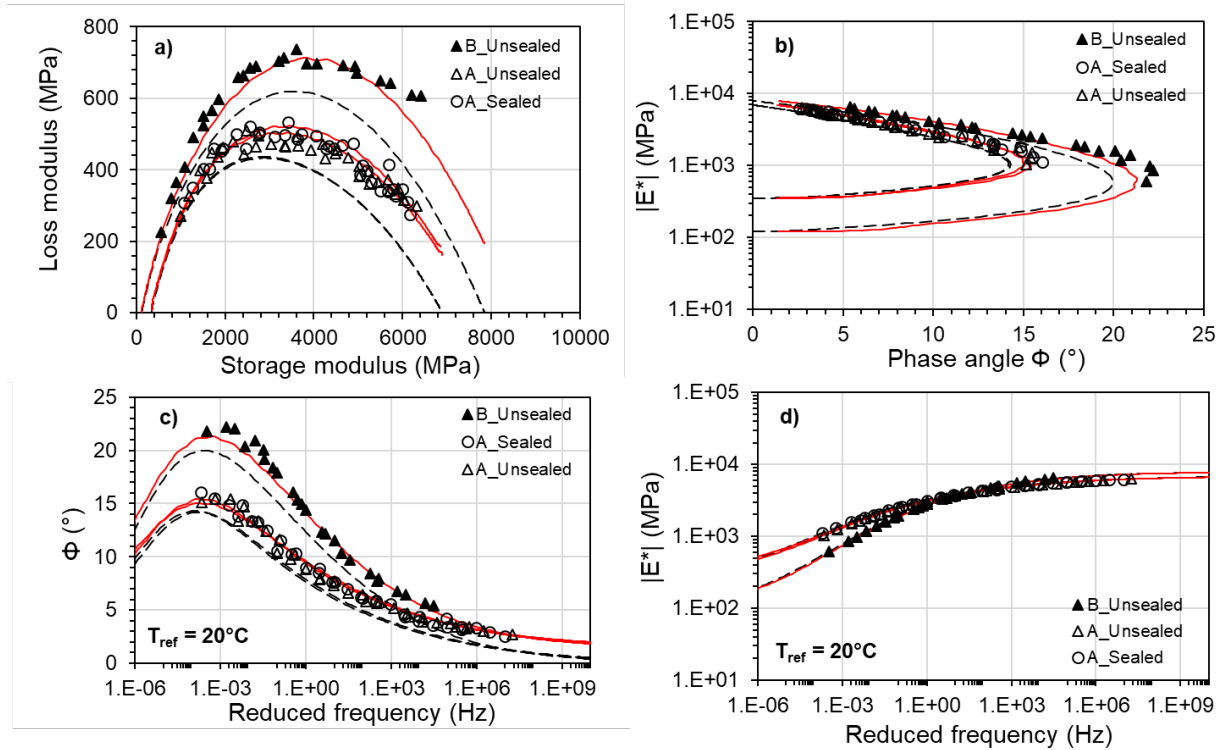


Figure 15 Application of the 2S2P1D (dashed line) and DBN (continuous line) models to the studied mixtures ($n = 40$): a) Cole-Cole plan, b) Black space, c) phase angle master curve and, d) complex modulus master curve ($T_{ref} = 20\text{ }^{\circ}\text{C}$)

5 DISCUSSION

Figure 16 shows the accuracy of 2S2P1D and DBN models according to the experimental data for the whole frequency and temperature ranges. The best fitting in both plans of the DBN model compared to the 2S2P1D are highlighted: norm of the complex modulus ($\pm 5\%$) and phase angle ($\pm 2^\circ$).

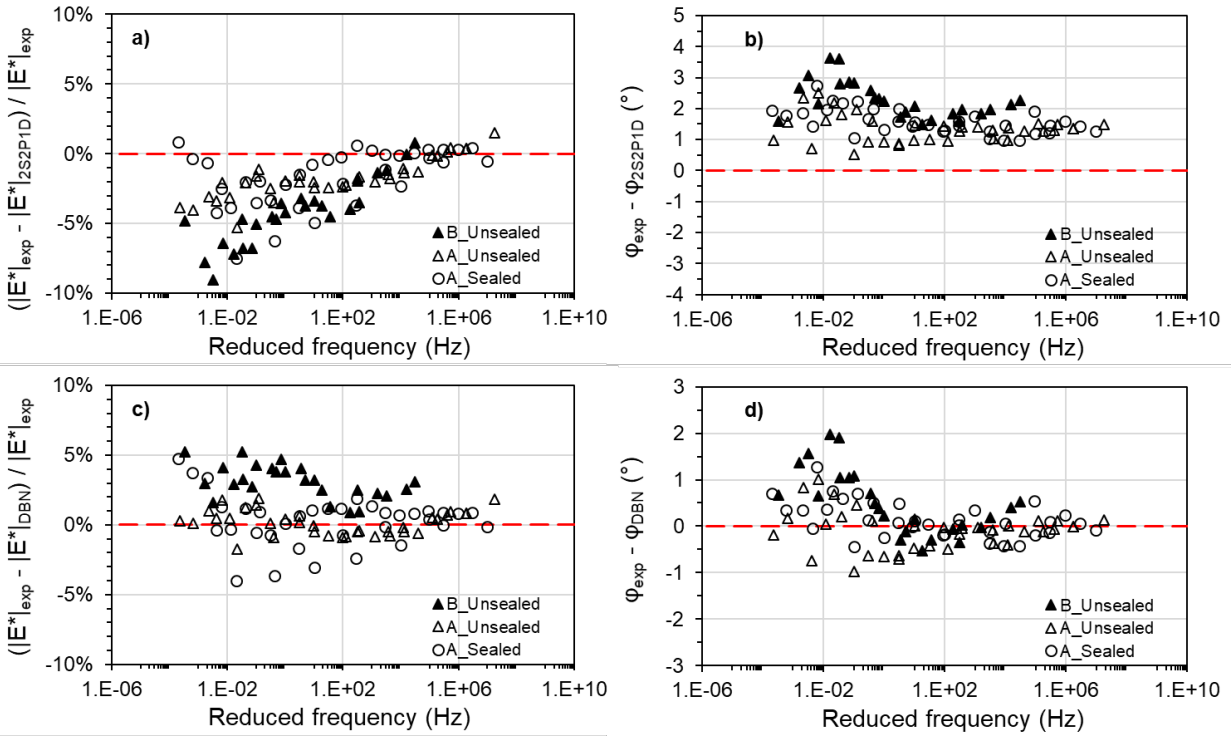


Figure 16 Accuracy of the model applied: a) 2S2P1D on the norm of complex modulus, b) 2S2P1D on the phase angle, c) DBN on the norm of complex modulus, and d) DBN on the phase angle

Table 5 lists the model parameters related to the DBN model and the modified version of the Huet-Sayegh model (Eq. 3). It is highlighted that the same values can be used by both approaches, even if the parameter β needs to be defined in case of DBN model. However, such high values make the contribution given by the dashpot almost negligible. This shows that the two approaches are able to fit the experimental data adopting the same parameters, but only in the case of DBN the material is represented by a rheological model which can be fully applied in the time domain and for higher strain rate (out of the LVE field).

Table 5 Rheological modelling parameters for the studied mixtures

Mixture	Model	E_{00} (MPa)	E_0 (MPa)	k (-)	h (-)	δ (-)	β (-)	τ_E (20°C) (-)	φ_{EP} (°)	φ_{AEP} (°)
A_Unsealed	DBN	350	6,900	0.14	0.37	2.25	10E+10	15.0	1.3	-
	HS _q	350	6,900	0.14	0.37	2.25	-	15.0	-	1.3
A_Sealed	DBN	350	6,900	0.14	0.37	2.25	10E+10	20.0	1.3	-
	HS _q	350	6,900	0.14	0.37	2.25	-	20.0	-	1.3
B_Unsealed	DBN	120	7,850	0.18	0.39	2.65	10E+05	2.5	1.4	-
	HS _q	120	7,850	0.18	0.39	2.65	-	2.5	-	1.4

Comparing parameters for mixes A_Unsealed and A_Sealed it is observed that the same are adopted, meaning that the sealed curing prevented further curing and ageing of the mixtures. The first two curing periods for a total of 28 days (14 days at 25 °C and 14 days at 40 °C) were enough to reach a stable condition of the material properties, which were not affected by ageing as much. The most important factor that affected the rheology of CBTM mixtures was the different emulsion (i.e. different residual bitumen) used to produce the mixtures. In particular, important differences could be highlighted comparing model parameters for mixes A_Unsealed and B_Unsealed. Bitumen from Emulsion B conferred to the CBTM mixture a higher modulus value at high frequencies (or low temperatures) and lower modulus at low frequencies (or high temperatures), which means a global higher temperature dependency. Moreover, the parameters related to the viscous part of the model k , h , δ are lower for mixture A_Unsealed, highlighting the fact that bitumen from Emulsion A gives a less viscous response compared to Emulsion B. The same conclusion can be confirmed by the values of the characteristic time τ_E . Generally, the higher the value of τ_E , the lower is the viscous contribution given by the binder. From these results, the difference between Emulsion A and B is one order of magnitude.

The non-viscous parameter φ_{EP} is almost the same for curing confinement and emulsion used, meaning that it does not depend on the residual bitumen and confirming that the curing confinement did not change the rheological response of mixtures. Being a parameter used to represent frictional or slightly plastic phenomena it is reasonable to assume that it could depend on the air voids content, bitumen dosage and/or the type of aggregates used. However, it is believed that the effect of non-viscous dissipation is reversible for a small number of cycles. Since these aspects were not analyzed in this study, further work is needed to clarify the role of the non-viscous component in CBTM mixtures.

6 CONCLUSIONS

This paper deals with the thermo-rheological modelling of CBTM mixtures in the small strain domain. An innovative approach is proposed employing the visco-plastic model DBN proposed in the literature. The paper focuses on the description of the DBN model application to CBTM materials; however, the new approach was applied to preliminarily study the effects of curing confinement type and emulsion source in the long-term properties of the CBTM mixtures studied. The following conclusions can be drawn:

- DBN is a suitable rheological model to well represent the thermo-rheological behaviour of cement-bitumen treated materials (CBTM) in the small strain domain. With 8 parameters it is possible to include in the same model both viscous and non-viscous responses obtaining an optimal fitting of the experimental results. The equivalent phase angle, φ_{EP} , represents a non-viscous dissipation parameter typically observed at higher levels of deformation, but useful in this study to consider frictional and/or plastic phenomena for the CBTM mixtures. From the results obtained, the φ_{EP} does not seem to depend on binder type and curing procedure. Using a different model would bring to the definition of different parameters (of stiffness and dissipation) which could lead to a misunderstanding of the material properties. This would bring to mistakes if more mixtures are compared (for example effect of air voids, gradation, bitumen type, etc.). Furthermore, the DBN model can be extended in the time domain, in order to characterize the material also at higher deformation rates (fatigue). Additional work is needed to improve the knowledge with regards to such new aspects in cold materials;
- Mixtures were cured for 14 days at 25 °C and 14 days at 40 °C in unsealed conditions. After that, a curing process of 11 months in sealed and unsealed conditions was followed, after which rheological properties were measured. Results showed that in both conditions the same stiffness was reached, meaning that the evolution of properties was not probably influenced by sealed or unsealed curing. It can be assumed that in sealed condition stiffness evolution was slowed down or stopped. The same mixture composition was employed to produce CBTM mixtures with two different emulsion sources, hence different residual binder. The emulsions chosen are present in the market as specific for cold recycling projects and they have the same raw characteristics: cationic, slow-setting emulsions with unmodified

binder. Nonetheless, results obtained are significantly affected by the type of residual bitumen, meaning that it is not an aspect that should be neglected in the mix design.

Future studies should focus on improving the application of the DBN model for cold materials to enhance the currently missing scientific knowledge of the material. In particular, attention should be dedicated to the deeper understanding of the elastoplastic dissipation and the variables that could affect such property. Moreover, a study focused on the repeatability of the CBTM complex modulus testing on a larger number of specimens and the following application of the DBN model would improve the fundamental knowledge of such materials and the suitability of the model proposed.

7 APPENDIX A

Table A.1 Generalized Kelvin-Voigt (GKV) parameters for 40 elements

Element	A_Unsealed		A_Sealed		B_Unsealed	
n	E _i	η _i	E _i	η _i	E _i	η _i
0	6.90E+03	-	6.85E+03	-	7.85E+03	-
1	2.73E+06	1.92E-12	3.35E+06	2.35E-12	8.64E+06	6.08E-12
2	4.28E+06	1.33E-11	5.17E+06	1.61E-11	1.23E+07	3.82E-11
3	2.90E+06	3.99E-11	3.54E+06	4.87E-11	9.43E+06	1.30E-10
4	2.97E+06	1.81E-10	3.76E+06	2.29E-10	1.31E+07	7.95E-10
5	3.86E+06	1.04E-09	4.76E+06	1.28E-09	7.62E+06	2.05E-09
6	2.57E+06	3.06E-09	2.96E+06	3.52E-09	7.00E+06	8.33E-09
7	2.40E+06	1.26E-08	2.88E+06	1.51E-08	4.66E+06	2.45E-08
8	1.75E+06	4.07E-08	2.00E+06	4.66E-08	3.96E+06	9.21E-08
9	1.55E+06	1.59E-07	1.81E+06	1.86E-07	2.79E+06	2.87E-07
10	1.18E+06	5.34E-07	1.33E+06	6.06E-07	2.27E+06	1.03E-06
11	1.01E+06	2.02E-06	1.15E+06	2.32E-06	1.66E+06	3.33E-06
12	7.84E+05	6.97E-06	8.79E+05	7.81E-06	1.31E+06	1.17E-05
13	6.58E+05	2.59E-05	7.40E+05	2.91E-05	9.77E+05	3.84E-05
14	5.21E+05	9.06E-05	5.76E+05	1.00E-04	7.63E+05	1.33E-04
15	4.32E+05	3.32E-04	4.77E+05	3.67E-04	5.73E+05	4.41E-04
16	3.45E+05	1.17E-03	3.76E+05	1.28E-03	4.43E+05	1.51E-03

17	2.84E+05	4.27E-03	3.08E+05	4.63E-03	3.35E+05	5.04E-03
18	2.28E+05	1.52E-02	2.45E+05	1.63E-02	2.57E+05	1.71E-02
19	1.86E+05	5.48E-02	1.99E+05	5.85E-02	1.95E+05	5.72E-02
20	1.50E+05	1.95E-01	1.59E+05	2.06E-01	1.48E+05	1.93E-01
21	1.22E+05	7.00E-01	1.28E+05	7.36E-01	1.12E+05	6.44E-01
22	9.78E+04	2.49E+00	1.02E+05	2.59E+00	8.47E+04	2.15E+00
23	7.88E+04	8.86E+00	8.17E+04	9.17E+00	6.35E+04	7.13E+00
24	6.29E+04	3.12E+01	6.46E+04	3.21E+01	4.74E+04	2.36E+01
25	5.00E+04	1.10E+02	5.12E+04	1.12E+02	3.51E+04	7.71E+01
26	3.92E+04	3.81E+02	4.00E+04	3.89E+02	2.57E+04	2.50E+02
27	3.05E+04	1.31E+03	3.11E+04	1.34E+03	1.86E+04	7.99E+02
28	2.34E+04	4.44E+03	2.39E+04	4.53E+03	1.33E+04	2.52E+03
29	1.77E+04	1.48E+04	1.81E+04	1.52E+04	9.34E+03	7.85E+03
30	1.31E+04	4.87E+04	1.36E+04	5.05E+04	6.47E+03	2.40E+04
31	9.64E+03	1.58E+05	1.01E+04	1.66E+05	4.43E+03	7.27E+04
32	7.05E+03	5.12E+05	7.53E+03	5.47E+05	3.01E+03	2.19E+05
33	5.21E+03	1.67E+06	5.66E+03	1.82E+06	2.06E+03	6.61E+05
34	3.99E+03	5.66E+06	4.39E+03	6.23E+06	1.45E+03	2.06E+06
35	3.27E+03	2.05E+07	3.61E+03	2.26E+07	1.08E+03	6.80E+06
36	2.98E+03	8.28E+07	3.24E+03	9.00E+07	9.05E+02	2.51E+07
37	3.10E+03	3.80E+08	3.27E+03	4.01E+08	8.81E+02	1.08E+08
38	3.62E+03	1.97E+09	3.65E+03	1.98E+09	1.02E+03	5.54E+08
39	4.55E+03	1.09E+10	4.34E+03	1.04E+10	1.37E+03	3.28E+09
40	4.37E+03	4.64E+10	3.64E+03	3.86E+10	9.48E+02	1.01E+10

537

538 8 REFERENCES

539 ARRA. (2001). *Basic asphalt recycling manual*.

540 ARRA. (2016). Recommended Construction Guidelines For Cold In-place Recycling (CIR) Using
541 Bituminous Recycling Agents.

542 Ashmawy, A. K., Salgado, R., Guha, S., & Drnevich, V. P. (1995). Soil damping and its use in
543 dynamic analyses.

544 Asphalt Academy, A. (2009). *Technical Guideline (TG2): Bitumen Stabilised Materials*.

545 Attia, T. (2020). *Interfaces between pavement layers in bituminous mixtures*. (Doctor of
546 Philosophy), École Nationale des Travaux Publics de l'État.

547 Blanc, M., Di Benedetto, H., & Tiouajni, S. (2011). Deformation characteristics of dry Hostun
548 sand with principal stress axes rotation. *Soils and foundations*, 51(4), 749-760.

549 Bocci, M., Grilli, A., Cardone, F., & Graziani, A. (2011). A study on the mechanical behaviour of
550 cement-bitumen treated materials. *Construction and Building Materials*, 25(2), 773-778.
551 doi: 10.1016/j.conbuildmat.2010.07.007

552 Cardone, F., Grilli, A., Bocci, M., & Graziani, A. (2014). Curing and temperature sensitivity of
553 cement-bitumen treated materials. *International Journal of Pavement Engineering*,
554 16(10), 868-880. doi: 10.1080/10298436.2014.966710

555 Carret, J.-C., Pedraza, A., Di Benedetto, H., & Sauzeat, C. (2018). Comparison of the 3-dim linear
556 viscoelastic behavior of asphalt mixes determined with tension-compression and dynamic
557 tests. *Construction and Building Materials*, 174, 529-536.

558 Chen, T., Luan, Y., Ma, T., Zhu, J., Huang, X., & Ma, S. (2020). Mechanical and microstructural
559 characteristics of different interfaces in cold recycled mixture containing cement and
560 asphalt emulsion. *Journal of Cleaner Production*, 120674.

561 Chomicz-Kowalska, A., & Maciejewski, K. (2020). Performance and viscoelastic assessment of
562 high-recycle rate cold foamed bitumen mixtures produced with different penetration
563 binders for rehabilitation of deteriorated pavements. *Journal of Cleaner Production*,
564 120517.

565 Dal Ben, M., & Jenkins, K. J. (2014). Performance of cold recycling materials with foamed
566 bitumen and increasing percentage of reclaimed asphalt pavement. *Road Materials and
567 Pavement Design*, 15(2), 348-371. doi: 10.1080/14680629.2013.872051

568 Di Benedetto, H., Blanc, M., Tiouajni, S., & Ezaoui, A. (2014). Elastoplastic model with loading
569 memory surfaces (LMS) for monotonic and cyclic behaviour of geomaterials. *International
570 Journal for Numerical and Analytical Methods in Geomechanics*, 38(14), 1477-1502.

571 Di Benedetto, H., Delaporte, B., & Sauzéat, C. (2007). Three-dimensional linear behavior of
572 bituminous materials: experiments and modeling. *International Journal of Geomechanics*,
573 7(2), 149-157.

574 Di Benedetto, H., Mondher, N., Sauzéat, C., & Olard, F. (2007). Three-dimensional thermo-
575 viscoplastic behaviour of bituminous materials: the DBN model. *Road Materials and
576 Pavement Design*, 8(2), 285-315.

577 Di Benedetto, H., Olard, F., Sauzéat, C., & Delaporte, B. (2004). Linear viscoelastic behaviour of
578 bituminous materials: From binders to mixes. *Road Materials and Pavement Design*,
579 5(sup1), 163-202.

580 Ferry, J. D. (1980). *Viscoelastic properties of polymers*: John Wiley & Sons.

581 Gandi, A., Carter, A., & Singh, D. (2017). Rheological behavior of cold recycled asphalt materials
582 with different contents of recycled asphalt pavements. *Innovative Infrastructure Solutions*,
583 2(1), 45.

584 Gayte, P. (2016). *Modélisation du comportement thermo-viscoplastique des enrobés bitumineux*.

585 Gayte, P., Di Benedetto, H., Sauzéat, C., & Nguyen, Q. T. (2016). Influence of transient effects
586 for analysis of complex modulus tests on bituminous mixtures. *Road Materials and*
587 *Pavement Design*, 17(2), 271-289.

588 Genta, G. (2009). *Vibration dynamics and control*: Springer.

589 Gergesova, M., Zupančič, B., Saprunov, I., & Emri, I. (2011). The closed form tTP shifting (CFS)
590 algorithm. *Journal of Rheology*, 55(1), 1-16.

591 Giani, M. I., Dotelli, G., Brandini, N., & Zampori, L. (2015). Comparative life cycle assessment
592 of asphalt pavements using reclaimed asphalt, warm mix technology and cold in-place
593 recycling. *Resources, Conservation and Recycling*, 104, 224-238. doi:
594 10.1016/j.resconrec.2015.08.006

595 Godenzoni, C., Graziani, A., & Bocci, M. (2015). *Influence of reclaimed asphalt content on the*
596 *complex modulus of cement bitumen treated materials*. Paper presented at the 6th
597 International conference bituminous mixtures and pavements, Thessaloniki (Greece).

598 Godenzoni, C., Graziani, A., & Perraton, D. (2016). Complex modulus characterisation of cold-
599 recycled mixtures with foamed bitumen and different contents of reclaimed asphalt. *Road*
600 *Materials and Pavement Design*, 18(1), 130-150. doi: 10.1080/14680629.2016.1142467

601 Graziani, A., Iafelice, C., Raschia, S., Perraton, D., & Carter, A. (2018). A procedure for
602 characterizing the curing process of cold recycled bitumen emulsion mixtures.
603 *Construction and Building Materials*, 173, 754-762.

604 Graziani, A., Mignini, C., Bocci, E., & Bocci, M. (2020). Complex Modulus Testing and
605 Rheological Modeling of Cold-Recycled Mixtures. *Journal of Testing and Evaluation*,
606 48(1), 20180905. doi: 10.1520/jte20180905

607 Grilli, A., Graziani, A., Bocci, E., & Bocci, M. (2016). Volumetric properties and influence of
608 water content on the compactability of cold recycled mixtures. *Materials and Structures*,
609 49(10), 4349-4362. doi: 10.1617/s11527-016-0792-x

610 Grilli, A., Graziani, A., & Bocci, M. (2012). Compactability and thermal sensitivity of cement-
611 bitumen-treated materials. *Road Materials and Pavement Design*, 13(4), 599-617. doi:
612 10.1080/14680629.2012.742624

613 Hodgkinson, A., & Visser, A. T. (2004). *The role of fillers and cementitious binders when*
614 *recycling with foamed bitumen or bitumen emulsion*. Paper presented at the 8th Conference
615 on Asphalt Pavements for Southern Africa, Sun City, South Africa.

616 Kim, Y., Im, S., & Lee, H. D. (2011). Impacts of Curing Time and Moisture Content on
617 Engineering Properties of Cold In-Place Recycling Mixtures Using Foamed or Emulsified
618 Asphalt. *Journal of Materials in Civil Engineering*, 23(5), 542-553. doi:
619 10.1061/(asce)mt.1943-5533.0000209

620 Lamothe, S., Perraton, D., & Benedetto, H. D. (2017). Degradation of hot mix asphalt samples
621 subjected to freeze-thaw cycles and partially saturated with water or brine. *Road Materials*
622 *and Pavement Design*, 18(4), 849-864. doi: 10.1080/14680629.2017.1286442

623 Lauter, K. A., & Corbett, M. A. (1998). *Developing gyratory compacter guidelines for use with*
624 *cold in-place recycled material*. Paper presented at the Proceedings of the... Annual
625 conference of canadian technical asphalt association.

626 Neifar, M., & Di Benedetto, H. (2001). Thermo-viscoplastic law for bituminous mixes. *Road*
627 *Materials and Pavement Design*, 2(1), 71-95.

628 Olard, F., & Di Benedetto, H. (2003). General “2S2P1D” model and relation between the linear
629 viscoelastic behaviours of bituminous binders and mixes. *Road Materials and Pavement*
630 *Design*, 4(2), 185-224.

631 Omrani, M. A., & Modarres, A. (2018). Emulsified cold recycled mixtures using cement kiln dust
632 and coal waste ash-mechanical-environmental impacts. *Journal of Cleaner Production*,
633 199, 101-111.

634 Pronk, A. C. (2006). The Huet-Sayegh Model; A simple and excellent rheological model for
635 master curves of asphalt mixes. *Asphalt Concrete*, 73-82.

636 Raschia, S., Graziani, A., Carter, A., & Perraton, D. (2019). Laboratory mechanical
637 characterisation of cold recycled mixtures produced with different RAP sources. *Road*
638 *Materials and Pavement Design*, 20(sup1), S233-S246. doi:
639 10.1080/14680629.2019.1588775

640 Raschia, S., Perraton, D., Graziani, A., & Carter, A. (2020). Influence of low production
641 temperatures on compactability and mechanical properties of cold recycled mixtures.
642 *Construction and Building Materials*, 232, 117169.

643 Saleh, M. F. (2007). Effect of rheology on the bitumen foamability and mechanical properties of
644 foam bitumen stabilised mixes. *International Journal of Pavement Engineering*, 8(2), 99-
645 110.

646 Stroup-Gardiner, M. (2011). *Recycling and Reclamation of Asphalt Pavements Using In-Place*
647 *Methods*.

648 Tatsuoka, F., Di Benedetto, H., Kongkitkul, W., Kongsukprasert, L., Nishi, T., & Sano, Y. (2008).
649 Modelling of ageing effects on the elasto-viscoplastic behaviour of geomaterial. *Soils and*
650 *foundations*, 48(2), 155-174.

651 Tiouajni, S., Di Benedetto, H., Sauzéat, C., & Pouget, S. (2011). Approximation of linear
652 viscoelastic model in the 3 dimensional case with mechanical analogues of finite size:
653 application to bituminous materials. *Road Materials and Pavement Design*, 12(4), 897-
654 930.

655 Zhu, C., Zhang, H., Huang, L., & Wei, C. (2019). Long-term performance and microstructure of
656 asphalt emulsion cold recycled mixture with different gradations. *Journal of Cleaner*
657 *Production*, 215, 944-951.

658

659